4H-SiC Nano-Pillar Avalanche Photodiode With Illumination-Dependent Characteristics

Rongdun Hong, Yi Zhou, Kang Long Wang, and Zhengyun Wu

***Abstract*—A 4H-SiC nano-pillar-based avalanche photodiode (NAPD) with a separate absorption region and a multiplication region is proposed and its optoelectronic performance is modeled. By properly designing the device geometry and the doping concentration of each layer, the avalanche breakdown voltage $(V_{\rm br})$ of the NAPD is found to be dependent of the incident wavelength and power density, which are explained by the band diagrams of 4H-SiC NAPDs.**

***Index Terms*—Avalanche, 4H-SiC, nano-pillar, photodiode.**

THE detection of light at ultraviolet (UV) wavelengths has special interests in a number of broad areas, including environmental monitoring, space research, military systems and medical applications [1]. Currently, photomultiplier tubes (PMT) are widely used due to their high responsivity and high internal gain $(> 10^6)$. However these devices are typically bulky, fragile and expensive, which leaves a room for developing alternative semiconductor-based technologies. Competing material systems include Si, III–V compounds such as (Al)GaN and SiC, which have all shown their promising aspects as well as challenges. However, SiC has emerged as an attractive candidate for UV detection due to its advantageous material properties over Si, such as wider bandgap, higher thermal conductivity, superior radiation hardness and higher quantum efficiency [2]. Although the recent freestanding GaN substrate has less dislocations than SiC substrates [3], compared to high Al content (Al)GaN with freestanding GaN substrate for visible-blind performance, SiC benefits from the availability of high ionization coefficient ratio, low cost, and mature processing technologies. Recently, significant progress has been made in fabricating SiC-based UV APD. Xin *et al.* have demonstrated 4H-SiC UV APD with the single photon counting capability at room temperature [4]. By employing the separated-absorption-multiplication (SAM) structure, Guo *et al.* have demonstrated 4H-SiC APD with 83% external quantum efficiency at 278 nm wavelength and a gain greater than 1000 [5]. However, due to the defect density of the SiC epitaxial films of SiC-based APD, the high defect density eventually limits the device size since the defects within the active APD area will ultimately lead to localized premature breakdown, instability and spatial nonuniformities in photoresponse [6]. 4H-SiC APD arrays based on small diameter elements have been proposed and demonstrated with the motivation that bad array elements could be disconnected and the catastrophic breakdown by localized defects could be prevented [6].

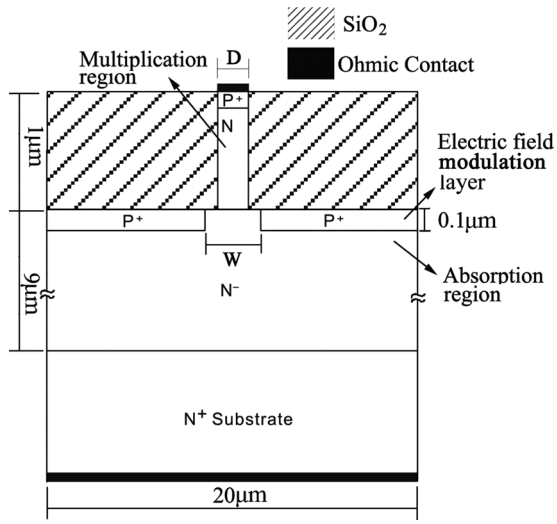

Fig. 1. Structure of 4H-SiC nano-pillar APD.

In this letter, we propose a 4H-SiC nano-pillar APD (NAPD) structure, featuring a nano-pillar multiplication region separated from a larger bulk absorption region. The nano-pillar for multiplication is designed as small as 0.3 μm in diameter so that the yield of defect-free array element can be maximized for APD array application. A comprehensive two-dimensional modeling tool was employed to simulate the device characteristics.

The device modeling was done using the ATLAS software package from SILVACO. The physical models and material parameters employed in this simulation are based on H. Cha's report, which optimize the electrical and optical modeling of 4H-SiC APD [7]. The governing physical models include ANALYTIC, FLDMOB, KLASRH, and SELB, which specifies the doping-dependent and temperature-dependent low field mobility, the electric-field-dependent mobility, the doping-dependent and temperature-dependent carriers' lifetime and SRH recombination, and the ionization rate physical model. Moreover, the carriers surface recombination velocity is specified by the INTERFACE command in the ALTAS program.

A typical device structure used for our modeling is shown in Fig. 1, which features a nano-pillar multiplication region in the center and a large bulk absorption region underneath. The entire device is 20.0 μm wide and built on an $N+$ substrate.

Manuscript received October 26, 2010; revised March 25, 2011; accepted April 02, 2011. Date of publication April 07, 2011; date of current version May 25, 2011.

R. Hong and Z. Wu are with Physics and Mechanical and Electrical Engineering, Xiamen University, Xiamen, 361005, Fujian, China (e-mail: rongdun_hong@hotmail.com; zhywu@xmu.edu.cn).

Y. Zhou and K. L. Wang are with the Electrical Engineering Department, University of California, Los Angeles, CA 90095 USA (e-mail: yizhou@ee.ucla.edu; wang@ee.ucla.edu).

Digital Object Identifier 10.1109/LPT.2011.2140391

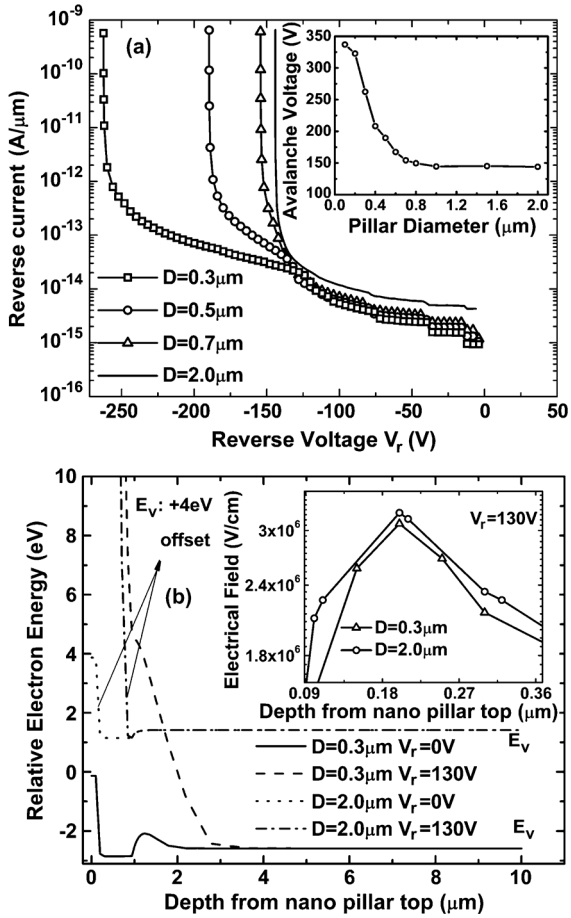

Fig. 2. (a) Simulated dark reverse I–V characteristics of 4H-SiC NAPD with different pillar diameter (D), in which the inset shows the avalanche voltage dependence of D; (b) simulated valence band diagrams and electric field intensity (inset) along the vertical direction of the device (in the middle of the device) for 4H-SiC NAPD with 0.3- and 2.0-μm pillar diameter, under 0- and 130-V reverse biases, in which the valence band diagrams for $D = 2.0$ μm are offset by 4 eV.

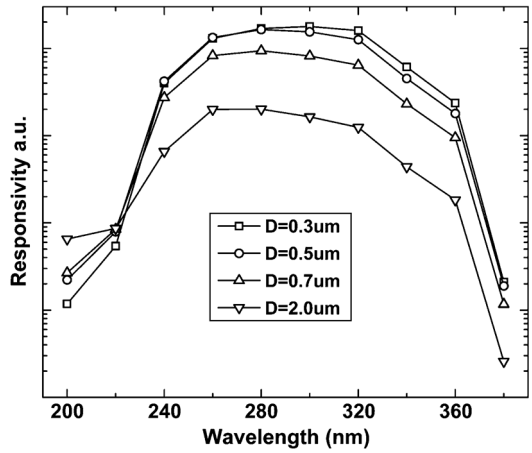

Fig. 3. Simulated spectral responsivities of 4H-SiC NAPD with different pillar diameter (D), under 1.0×10^{-2} W/cm^2 illumination. The bias of NAPD is the $95\% \times V_{\rm br}$ of the NAPD under 1.0×10^{-2} W/cm^2 illumination with wavelength of 280 nm.

The absorption region contains a 9 μm thick $N-$ layer and a 0.1 μm thick $P+$ layer on both shoulders, which can modulate the electric field intensity in the pillar. The space between these two $P+$ shoulders (W) is always 0.4 μm wider than the pillar diameter (D). The pillar is 1.0 μm in height. Within the pillar, from top to bottom, it contains a 0.2 μm thick $P+$ layer and a 0.8 μm thick N-type multiplication layer. A 1.0 μm thick SiO_2 layer is used as the passivation layer. The doping level for $P+$, N, $N-$ and $N+$ layers are 1.0×10^{19} cm$_3$, 2.4×10^{17}/cm$_3$, 2.0×10^{15}/cm^3 and 1.0×10^{19}/cm^3, respectively.

Fig. 2(a) shows the dark reverse bias I–V characteristics of 4H-SiC NAPDs with different pillar diameters (D) and the dependence of $V_{\rm br}$ on D (inset), which shows $V_{\rm br}$ decreases with D and eventually saturates to a value close to the avalanche voltage of conventional bulk 4H-SiC APD (about 144.1 V in our case). It is noted that D can be replaced by W in Fig. 2, for W is always 0.4 μm wider than D. The mechanism which leads to such a size dependent $V_{\rm br}$ of the 4H-SiC NAPD will be discussed below.

Fig. 2(b) shows the valence band diagrams of the 4H-SiC NAPD at the center of the pillar as a function of the distance away from the pillar top, with the pillar diameter of 0.3 μm and 2.0 μm, under the reverse bias of 0 V and 130 V, respectively. For the 0.3 μm pillar diameter NAPD under 0 V bias, the space between the $P+$ shoulders (W) is very small. Therefore there is a potential well for holes in the valence band in the pillar bottom, which is due to the $P+N-$ junction build-in electric field under the pillar. For the 2.0 μm pillar diameter NAPD, because W is much wider, the $P+N-$ junction build-in electric field can not cover completely the $N-$ region under the pillar and no potential well for holes exists in the bottom center of the pillar. Compared to the 2.0 μm pillar diameter NAPD, the depletion layer in the 0.3 μm pillar diameter pillar, due to the effect of potential well for holes, punches into the $N-$ layer at lower reverse bias voltage. Therefore, while the reverse biases are the same (130 V), the punch-through occurs only for the 0.3 μm pillar diameter NAPD but not the 2.0 μm pillar diameter one. Since, after punch-through, most of the increased reverse voltage will be dropped on the $N-$ layer for the 0.3 μm pillar diameter NAPD, the maximum electric field intensity ($E_{\rm max}$) inside the 0.3 μm pillar diameter NAPD will be lower than that of the 2.0 μm pillar diameter one, leading to $V_{\rm br}$ for the 0.3 μm pillar diameter NAPD will be much higher than that of the 2.0 μm pillar diameter one. The $E_{\rm max}$, under 130 V reverse bias, are 3.084×10^6 V/cm and 3.226×10^6 V/cm for 0.3 μm and 2.0 μm pillar diameter NAPDs, respectively (inset of Fig. 2(b)). Therefore, for small pillar diameter NAPD, the $P+N-$ junction build-in electric field under the pillar will suppress the avalanche of device. It should be noted that it's not the pillar diameter but the depleted region between the $P+$ shoulders, which modulates the electric field intensity inside the NAPD and causes this size dependent effect.

To observe clearly the effect of pillar diameter on the responsivity, the responsivity spectra of 4H-SiC NAPD with different D (under 1.0×10^{-2} W/cm^2 illumination) were shown in Fig. 3. The bias of NAPD is $95\% \times V_{\rm br}$ of the NAPD under 1.0×10^{-2} W/cm^2 illumination with wavelength of 280 nm. The illumination is incident vertically above the device and covers

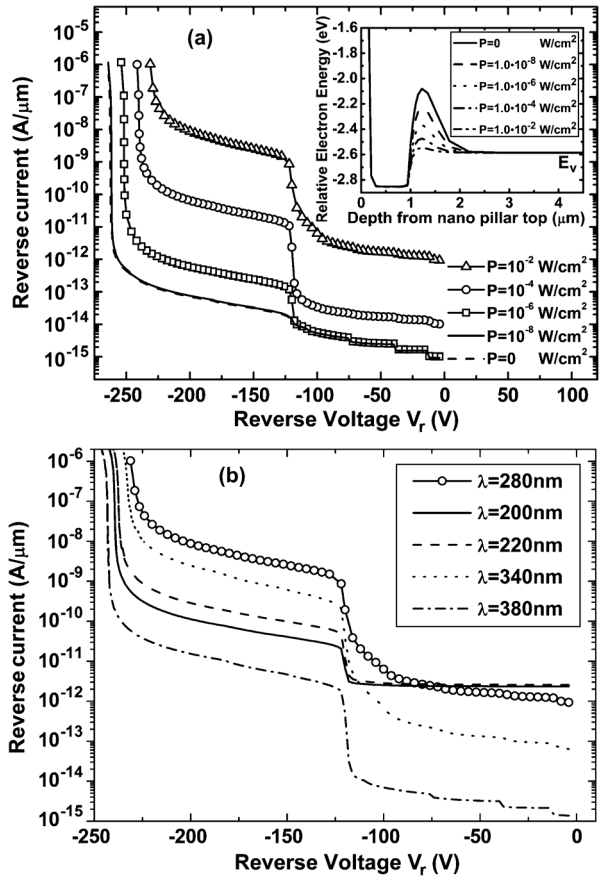

Fig. 4. (a) Simulated I–V characteristics of 4H-SiC NAPD under illumination with different power densities at $\lambda = 280$ nm and (b) with different wavelengths under 1.0×10^{-2} W/cm^2 illumination. The avalanche voltage and band diagram of NAPD are dependent on power density and wavelength of the incident illumination.

the whole surface of the device. Fig. 3 illustrates that as D decreases, the responsivity peak of 4H-SiC NAPD increases and has red-shift, which can be understood by Fig. 2. The depletion region for the NAPD with smaller D expands deeper than that with larger D (Fig. 2(b)), which will cause more photon absorption for NAPD with smaller D under illumination with long wavelength. Then the responsivity peak of 4H-SiC NAPD will increase and have red-shift.

We will show that this modulation effect is also dependent on power density and wavelength of the incident illumination.

To achieve obvious illumination-dependent characteristics of NAPD, the photoresponse of the 4H-SiC NAPD of 0.3 μm pillar diameter is simulated under illumination with different power densities (P) and wavelengths (λ). The absorption coefficient of 4H-SiC as a function of wavelength has been well studied [7], which was employed in this work. Fig. 4(a) shows the reverse I–V characteristics of this device under illumination with $\lambda = 280$ nm and different P. Unlike the conventional bulk APD, which has a $V_{\rm br}$ independent of P, the 4H-SiC NAPD shows an optical power density dependent $V_{\rm br}$, which decreases with P. Although, in Fig. 4(a), the I–V curve for $P = 1 \times 10^{-8}$ W/cm^2 almost overlaps the one without illumination, the $V_{\rm br}$ difference is still about 0.7 V. Such a unique photoresponse can be explained by the fact that the UV illumination results in a photovoltaic field at $P + N-$ junction, which is opposite to the $P + N-$ junction build-in electric field in the $N-$ region under the pillar and reduces the total electric field intensity of $P + N-$ junction, leading to the decreasing depth of the hole potential well (Inset of Fig. 4(a)) and decrease of $V_{\rm br}$ with P. Fig. 4(b) shows the reverse I–V characteristics of this NAPD under illumination with different λ and $P = 1.0 \times 10^{-2}$ W/cm^2. It is understandable that the photovoltaic field intensity is also a function of λ, for the different absorption coefficient. The photovoltaic field intensity reaches to the maximum at the wavelength ($\lambda \approx 280$ nm, in Fig. 4(b), for 4H-SiC) corresponding to the highest spectral responsivity. So, the $V_{\rm br}$ of NAPD under $\lambda = 280$ nm illumination will be the minimum.

In conclusion, we have demonstrated the design and modeling of a nano-pillar based 4H-SiC APD (NAPD) with a separate absorption and a multiplication (SAM) region. The band diagram, avalanche breakdown voltage and photoresponse of the NAPD are strongly dependent of the device geometry, incident UV wavelength as well as the incident UV power density. This 4H-SiC NAPD is promising to serve as the element for high performance UV array detectors.

REFERENCES

[1] J. C. Carrano, T. Li, P. A. Grudowski, R. D. Dupuis, and J. C. Campbell, "Improved detection of the invisible," *IEEE Circuits Devices Mag.*, vol. 15, no. 5, pp. 15–24, Sep. 1999.

[2] A. R. Powell and L. B. Rowland, "SiC Materials—Progress, Status & Potential Roadblocks," *Proc. IEEE*, vol. 90, no. 6, pp. 942–955, Jun. 2002.

[3] Z. Vashaei, E. Cicek, C. Bayram, R. McClintock, and M. Razeghi, "GaN avalanche photodiodes grown on m-plane freestanding GaN substrate," *Appl. Phys. Lett.*, vol. 96, pp. 201908–201908-3, May, 2010.

[4] X. Xin, F. Yan, X. Sun, P. Alexandrove, C. M. Stahle, J. Hu, M. Matsumura, X. Li, M. Weiner, and H. J. Zhao, "Demonstration of 4H-SiC visible-blind EUV and UV detector with large detection area," *Electron. Lett.*, vol. 41, no. 21, pp. 1192–1193, Oct. 2005.

[5] X. Guo, L. B. Rowland, G. T. Dunne, J. A. Fronheiser, P. M. Sandvik, A. L. Beck, and J. C. Campbell, "Demonstration of ultraviolet separate absorption and multiplication 4H-SiC avalanche photodiodes," *IEEE. Photon. Technol. Lett.*, vol. 18, no. 1, pp. 136–138, Jan. 1, 2006.

[6] X. Bai, D. McIntosh, H. Liu, and J. C. Campbell, "High single photon detection efficiency 4H-SiC avalanche photodiodes," *Proc. SPIE*, vol. 7320, p. 73200I-1, Apr. 2009.

[7] H. Cha and P. M. Sandvik, "Electrical and optical modeling of 4H-SiC avalanche photodiodes," *Jpn. J. Appl. Phys.*, vol. 47, no. 7, pp. 5423–5425, Jul. 2008.